Geophysical Research Letters

RESEARCH LETTER
10.1029/2019GL084744

Key Points:
- Temporal evolution of slip, foreshocks and fault coupling during laboratory earthquake nucleation depend on fluid pressure and slip history
- The observed precursory moment release during nucleation scales with the mainshock moment release independent of fault conditions
- A scaling relationship quantitatively predicts the experimental data. An extrapolation is proposed for natural earthquakes

Supporting Information:
- Supporting Information S1

Correspondence to:
M. Acosta,
mateo.acosta@epfl.ch

Citation:
Acosta, M., Passelègue, F. X., Schubnel, A., Madariaga, R., & Violay, M. (2019). Can precursory moment release scale with earthquake magnitude? A view from the laboratory. *Geophysical Research Letters*, *46*. https://doi.org/10.1029/2019GL084744

Received 5 AUG 2019
Accepted 6 NOV 2019
Accepted article online 11 NOV 2019

Can Precursory Moment Release Scale With Earthquake Magnitude? A View From the Laboratory

Mateo Acosta[1], François X. Passelègue[1], Alexandre Schubnel[2], Raúl Madariaga[2], and Marie Violay[1]

[1]EPFL, LEMR, Lausanne, Switzerland, [2]Laboratoire de Géologie, CNRS, UMR, ENS, Paris, France

Abstract Today, earthquake precursors remain debated. While precursory slow slip is an important feature of earthquake nucleation, foreshock sequences are not always observed, and their temporal evolution remains poorly constrained. We report on laboratory earthquakes conducted under upper-crustal stress and fluid pressure conditions. The dynamics of precursors (slip, seismicity, and fault coupling) prior to the mainshock are dramatically affected by slight changes in fault conditions (fluid pressure and slip history). A relationship between precursory moment release and mainshock magnitude is systematically observed, independent of fault conditions. Based on nucleation theory, we derive a semiempirical scaling relationship which explains this trend for laboratory earthquakes. Several natural observations of earthquakes ranging from ~M_w 6.0–9.0, where precursory moment release could be estimated, seem to follow the extrapolation of the laboratory-derived scaling law. Notwithstanding spatiotemporal complexity in natural seismicity, some moderate to large earthquake magnitudes might be estimated through integrated seismological and geodetic measurements of both seismic and aseismic slips during nucleation.

Plain Language Summary Understanding the preparation phase that precedes earthquake ruptures (nucleation) is crucial for seismic hazard assessment because it might provide information on the impending earthquake. Here, we show that the temporal evolution of laboratory earthquake precursors (precursory slow slip, precursory seismicity, and fault coupling) is of little use in assessing an impending earthquake's size. Nevertheless, independent of fault slip behavior (seismic or aseismic) and environmental conditions (stress state and fluid pressure and slip history), the amount of moment released during the preparation phase scales with the earthquake's magnitude. This property is demonstrated by laboratory observations and earthquake nucleation theory and seems compatible with several natural observations of earthquakes ranging from M_w 6.0 to M_w 9.0. As a consequence, if earthquakes exhibit a preparation phase, it could be possible that this phase is larger or longer for higher magnitude earthquakes and consequently, more likely to be detectable.

1. Introduction

The study of recent well-instrumented moderate and large magnitude earthquakes has highlighted that several ruptures were preceded by precursory slip, linked or not with foreshock sequences (Bouchon et al., 2013; Kato et al., 2012; Socquet et al., 2017; Tape et al., 2018; Voss et al., 2018). Theoretical and numerical models using either slip-weakening laws (Campillo & Ionescu, 1997; Ida, 1972; Ohnaka, 2010; Uenishi & Rice, 2003) or rate and state friction laws (Rubin and Ampuero, 2005; Lapusta & Rice, 2003; Noda et al., 2013; Dublanchet, 2018; Yabe & Ide, 2018) predict that earthquake rupture is preceded by a nucleation phase. Once the shear stress on the fault is high enough (corresponding to the static friction coefficient of the fault), a local patch of the fault (where the shear strength is lower than in its surroundings) begins to slip. The rupture accelerates over that growing fault patch until it reaches a characteristic length L_c, at which point dynamic rupture propagation initiates if enough elastic strain energy is dissipated at the rupture tip (Campillo & Ionescu, 1997; Ohnaka, 2010; Uenishi & Rice, 2003). Nucleation theory under slip-weakening laws predicts that L_c is a function of the earthquake's effective fracture energy (breakdown work) G' (Campillo & Ionescu, 1997; Uenishi & Rice, 2003), suggesting a link between earthquake nucleation and propagation. While the nucleation phase has been studied in the laboratory (Ben David et al., 2010; Byerlee & Summers, 1975; Dieterich, 1978; Latour et al., 2013; McLaskey & Lockner, 2014; Ohnaka, 2010; Passelègue et al., 2017; Scholz et al., 1972; Yamashita et al., 2018), natural observations of nucleation phases are scarce and remain debated.

In natural observations, two end-member models for nucleation coexist (Gomberg, 2018). First, the preslip model states that a background stable slip event triggers foreshocks until the main rupture can propagate (Tape et al., 2018). Second, the cascade model states that foreshocks trigger one another randomly up to the main rupture (Ellsworth & Bulut, 2018). To this day, nucleation remains unresolved because the temporal evolutions of earthquake precursors seem contradictory from one earthquake to another. In fact, observations of precursory slip prior to large magnitude earthquakes show different slip and foreshock evolutions up to the mainshock. As examples, for the 2011 M_w 9.0 Tohoku-Oki earthquake, Kato et al. (2012) observed foreshock acceleration and growth of the slipping zone followed by a seismic quiescence phase resulting in a large magnitude foreshock and the mainshock. On the other hand, Socquet et al. (2017) observed that an 8-month long slow slip event preceded a large foreshock and the 2014 M_w 8.1 Iquique earthquake. In general, temporal evolution of precursory slip and seismicity can be dramatically different for different earthquakes. This wide range of observations might be reconciled at the laboratory scale, where rupture propagation is recorded under well-controlled conditions.

Here, we closely study laboratory earthquake nucleation and propagation. We observe that, while the temporal evolution of precursors dramatically changes with variations in fault conditions, a straightforward relationship could link the precursory and coseismic moment release in the laboratory. We extrapolate this relationship to natural earthquakes.

2. Methods

Here, we carefully analyzed the nucleation phase of 150+ laboratory stick-slip events conducted under triaxial stress conditions (Supporting Information Figure S1a) representative of the upper seismogenic crust. Confining pressures (σ_3) ranged between 20 and 100 MPa and pore fluid pressures (p_f) from 0 to 60 MPa.

2.1. Experimental Setup

The samples were 30° saw cut Westerly granite cylinders of 40-mm diameter and 88-mm length (Figure S1c). Samples were first loaded isostatically (e.g., axial = radial effective stress) to the targeted σ_3 and p_f. They were then loaded at constant axial strain rates ~10^{-5} s^{-1}. During axial loading, p_f was kept constant at the target pressure. Far field (e.g., external to the confining chamber) axial and radial effective stresses (σ_1' and σ_3', respectively), p_f, and displacements were monitored at 100-Hz sampling frequency. Fault displacement was computed by projecting axial displacement corrected both from apparatus stiffness and sample elasticity. For details on the experimental methods and loading procedure, see Item S1 and Figures S1 and S2.

2.2. Acoustic Emission Monitoring

Piezoelectric acoustic emission (AE) sensors (15) were deployed on the sample. Sensors were monitored with two setups (Item S1). High amplification and sensor position (~1 mm away from the fault; Figure S1b) allowed for monitoring of the spontaneous microseismicity surging from the fault during deformation in a triggered mode at 10-MHz sampling frequency (Passelègue et al., 2017).

2.3. Near-Fault Stress Monitoring

Samples were instrumented to monitor near-fault stress evolution at low and high sampling frequency (100 Hz and 10 MHz) through 350-ohm strain gauges located ~1 mm away from the fault (Figure S1b). Sensor orientation allowed for the direct recording of differential strain further calibrated to differential stress ($\sigma_1 - \sigma_3$). Triggered sampling of near-fault differential stress allowed for good estimations of dynamic stress drops during the main ruptures in our experiments (Acosta et al., 2018; Passelègue et al., 2016).

3. Experimental Results

In sections 3.1–3.3, we present the experimental results for two experiments conducted at the same σ_3' where the only difference was p_f (one nominally dry, conducted under room humidity conditions and one at 1 MPa water fluid pressure). In section 3.4, we present the whole experimental data set compiled in Table S1. Hereafter, we assume that the main instabilities that give rise to sudden large stress drops and displacements are earthquake analogs (Brace & Byerlee, 1966). The observed frictional and seismic behavior of the fault preceding the main instabilities is therefore considered as part of the precursory nucleation phase (such assumption is further detailed in section 4.1 and Item S2).

3.1. Temporal Evolution of Stress and Slip Prior to the Mainshock

In all experiments, the displacement versus near fault stress curve (Figures 1a and 1d) revealed an initial elastic loading phase until a stress state τ_s, in agreement with static friction of rocks (Byerlee, 1978). Then, the fault started to slip in a slow, stable manner (Byerlee & Summers, 1975; Ohnaka, 2010; Scholz et al., 1972). When precursory slip (u_{prec}) finished, the fault's maximum shear strength (τ_0) was reached and the instability propagated with fast coseismic slip (u_{cos}) and a sudden stress drop ($\Delta\sigma$) down to a final stress value (τ_f). When coseismic slip arrested, as constant loading continued, a new elastic loading phase ensued, repeating the stick-slip cycle (Figure 1). Comparing a nominally dry experiment and an experiment conducted at 1 MPa water fluid pressure shows large differences in slip behavior prior to the main rupture. Under dry conditions (Figure 1b), u_{prec} (red curve) reached ~10 μm with a steady acceleration up to the mainshock. In the presence of 1 MPa water pressure, u_{prec} presented two different acceleration phases and reached ~20 μm before the mainshock.

3.2. Temporal Evolution of AE Precursors (Foreshocks)

Comparing the same experiments described in section 3.1, we observe that, in dry experiments, precursory slip is systematically related to AE occurrence (Figure 1b). Remarkably, AEs do not start from the beginning of the precursory slip acceleration but seem delayed in time until few seconds before the mainshock. Increasing cumulative fault displacement (subsequent stick-slip events) led to an increase of the total AEs recorded over single stick-slip cycles (from 31 in Cycle 1 to 79 in Cycle 10). Under all fluid pressurized conditions ($P_f = 1$ to 60 MPa), we recorded no AEs (Figure 1e) even though the triggering setup and sensor position was exactly the same as in dry experiments.

3.3. Fault (Un)Coupling Temporal Evolution During the Precursory Slip Phase

An important earthquake precursor is fault coupling (FC; Métois et al., 2012, Savage, 1983). Here, we computed FC as a function of time to mainshock during earthquake sequences recorded both in dry and 1 MPa water-pressurized conditions (Figure 1c and 1f, respectively). FC is defined as the ratio between the estimated fault slip rate to the imposed displacement rate when the fault is fully locked. Thus, we first computed the fault's slip rate ($\dot{u}_f$) recorded using external gap sensors with 1-s centered time windows such that

$$\dot{u_f}\ (t) = \frac{u(t + 0.5\ \mathrm{s}) - u(t - 0.5\ \mathrm{s})}{((t + 0.5\ \mathrm{s}) - (t - 0.5\ \mathrm{s}))}. \quad (1)$$

Due to fast strain rates imposed in our experiments compared to tectonic loading rates, we assumed that all deviations in strain rate from a fully coupled fault resulted from slip along the fault and not from bulk deformation of the surrounding rock (for details on this assumption, see Item S2 and Scholz et al., 1972; Byerlee & Summers, 1975). Then, we defined the mechanical coupling of the fault as the ratio between the estimated fault slip rate to the imposed displacement rate when the fault is fully coupled ($\dot{u}_0$; note that this is the displacement rate during fully elastic deformation of the entire sample) such that $\mathrm{FC} = \left(\frac{\dot{u}_f}{\dot{u}_0}\right)$. This estimation of the FC is comparable with the one derived from geodetic measurements along natural faults (Métois et al., 2012; Moreno et al., 2010; Savage, 1983). The evolution of FC directly reflects the rollover of the stress displacement curves (Figure S2).

As expected, the faults remained strong (FC ~ 1) during elastic loading. In dry conditions, at the onset of the mainshock, FC decreased to ~0.85–0.7 when u_{prec} accelerated. With subsequent events, FC at the onset of the mainshock decreased (Figure 1c, darkest traces). With pressurized fluids, FC decreased to ~0.5 at the onset of the mainshock. No influence of cumulative events (e.g., sliding history) was noted under pressurized fluid conditions (Figure 1f).

3.4. Magnitudes of the Precursory and Coseismic Stages

After applying a correction for the apparatus' and sample's elasticity, we compiled the precursory (all inelastic slip prior to the mainshock) and coseismic slips (all slip starting from the mainshock until the fault reloads in an elastic manner). Values are reported in Table S1. We suggest that the precursory slip recorded corresponds to all the inelastic displacement of the faults because i) the stress needed for fault reactivation in our experiments is considerably lower than the onset of bulk rock damage; ii) the frictional stress for fault

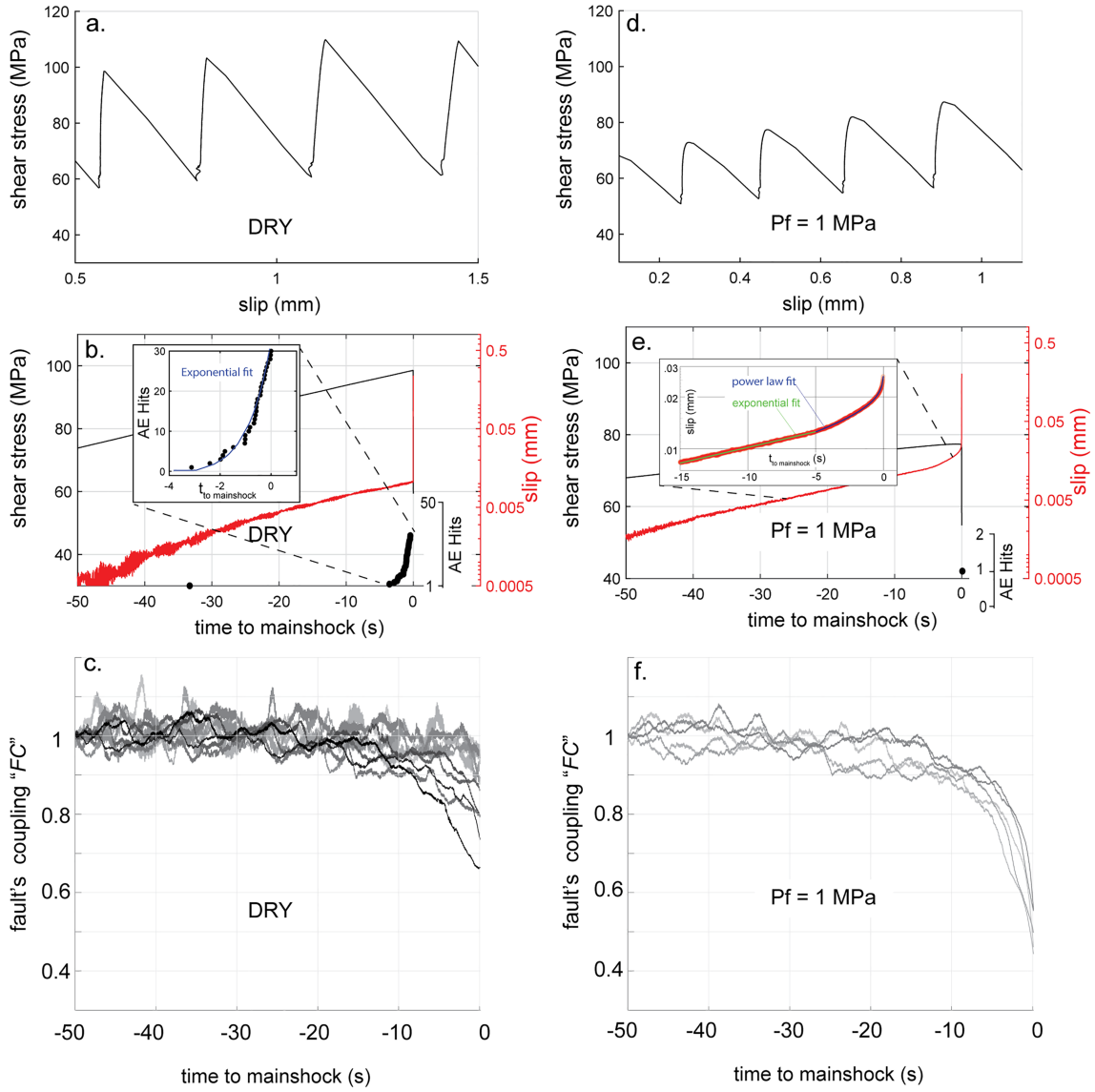

Figure 1. Stick-slip experiments and temporal evolution of earthquake precursors. (a–c) Dry experiment, and (d to f) experiment at fluid pressure $p_f = 1$ MPa. (a, d) Shear stress versus on-fault slip for experiments run at confining pressure $\sigma_3' = 70$ MPa. (b, e) Shear stress (black line), fault slip (red line in log scale), and AE's (black dots) for one stick-slip cycle versus time to mainshock ($0 = t_0$). Inset in b shows a close up of AE's from $t_0 - 4$ s with exponential fit. In d, the only acoustic emission arrival was the mainshock. Inset shows an exponential fit to the slip over time for the first nucleation stage from $t_0 - 15$ s to $t_0 - 5$ s as $u(t) = 0.015 \times \exp[(t_0 - t)/23.8]$ in green. In addition, in blue, a power law fit from $t_0 - 5$ s to t_0 as $u(t) = u(t_0 - 5\text{ s}) - 0.0116 \times t^{0.254}$. (c, f) Fault coupling versus time to mainshock for experiments at $\sigma_3' = 70$ MPa. The darkest traces correspond to later events. The fluctuations at long times before the mainshock can be due to slip and slip velocity measurements close to the sensor resolution.

reactivation corresponds to the static friction of rock (Byerlee, 1978); iii) no damage of the bulk was recorded while the faults' surfaces accommodated all the inelastic deformation; and iv) during the elastic loading phase, no AEs were recorded (for details, refer to Item S2). From Figure 2b, we can observe that u_{prec} ranges from ~1 to ~50 μm, and u_{cos} ranges from ~15 to ~350 μm.

As observed in previous studies (Acosta et al., 2018; Passelègue et al., 2016), the amount of slip induced during the coseismic stage is a function of the initial stress acting on the fault (Figure 2a, squares), independent of fluid pressure. The larger the initial shear stress, the larger the resulting static stress drop and u_{cos}. While this trend is expected due to the control by the stiffness of the apparatus, a similar relationship is observed for u_{prec} (Figure 2a, circles). Large coseismic events (i.e., bigger laboratory earthquakes) are consistently

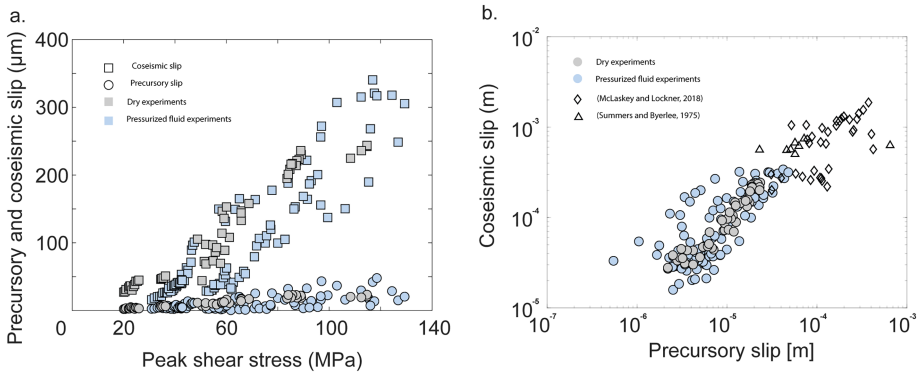

Figure 2. Compilation of experimental data. (a) Precursory (circles) and coseismic (squares) fault slips as a function of peak shear stress in our experiments. Blue filling accounts for experiments in the presence of fluid pressures and gray filling for nominally dry experiments. (b) Coseismic fault slip as a function of precursory slip. Filling is the same as in panel a. All other symbols account for external data reported in Table S2.

preceded by a larger u_{prec} than small coseismic events (Figure 2b). Note that this trend is clearer in dry experiments than in fluid-pressurized experiments because the presence of fluids and the initial fluid pressure modify coseismic weakening, that is, the energy budget of laboratory earthquakes (Acosta et al., 2018; Cornelio et al., 2019; Violay et al., 2013).

4. Discussion

4.1. Temporal Evolution of Earthquake Precursors

Our experimental results suggest that the magnitude of the precursory stage, and particularly the amount of slip released prior to the mainshock, could scale with the final coseismic slip, that is, the size of the earthquake which is going to rupture. Importantly, we observed that the growth of this u_{prec} over time is compatible with nucleation theory (Campillo & Ionescu, 1997; Uenishi & Rice, 2003; Ohnaka, 2010; Latour et al., 2013; Passelègue et al., 2016). In fact, in dry conditions, precursory slip evolves exponentially following $u_{prec}(t) = u_0 \times \exp[(t_0 - t)/t_c]$, where t_0 is the time of the mainshock, t_c the characteristic nucleation time (Latour et al., 2013), and u_0 is fault slip at the beginning of the acceleration phase (Figure 1b). In these conditions, the precursory stage exhibits foreshock activity, which also follows an exponential increase until t_0, consistent with the exponential acceleration of u_{prec}. In presence of fluids (Figure 1e), the nucleation phase is characterized by two clearly distinguishable slip acceleration stages. The first one is described by an exponential acceleration as observed in dry conditions. However, a transition from exponential growth to a power law in time is observed a few seconds prior to dynamic rupture propagation. This change in acceleration of u_{prec} is comparable to the nucleation process observed through high-speed photoelasticity in transparent polymers (Latour et al., 2013). One explanation of the absence of the second slip phase in dry experiments is that the acceleration stage can be short; potentially the reason why it was not observed. Further experimental work is needed to understand this behavior.

Surprisingly, under all fluid pressures, u_{prec} is not associated with any AEs. It is unlikely that the absence of foreshocks in all fluid-pressurized conditions results solely from an increased attenuation of seismic waves since the sensors were located <1 mm away from the fault. Previous experiments have indeed shown that AEs are systematically observed prior to the failure of intact or thermally cracked, dry or water saturated granite specimens (Wang et al., 2013). The absence of recorded foreshocks in all fluid-pressurized experiments might nevertheless be due to the high recording threshold of our AE triggered setup (0.001 V). Such a recording threshold can also possibly explain why AE bursts are recorded only a few seconds after the onset of precursory slip in dry conditions (Figure 1a). Nonetheless, in our experiments, foreshock occurrence and detection are clearly diminished in the presence of fluids. FC decreased with subsequent events in dry conditions. This could be due to fault surface evolution (e.g., gouge production and roughness change) as cumulative slip is accommodated by the fault (Scholz et al., 1972). With pressurized fluids, no influence of the sliding history and fault surface evolution was noted. Previous experiments (Cornelio et al., 2019;

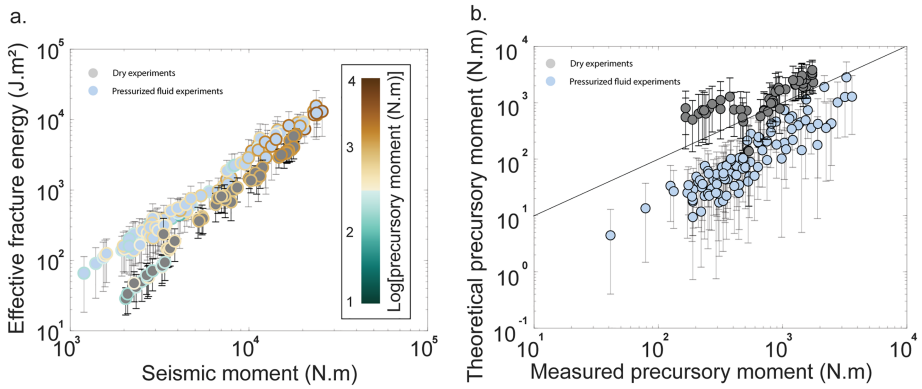

Figure 3. Precursory and coseismic moment release in laboratory earthquakes. (a) Effective fracture energy as a function of coseismic moment. Blue filling accounts for experiments in the presence of fluid pressures and gray filling for nominally dry experiments. Color bar accounts for the measured precursory moment in our laboratory earthquakes. Error bars show the upper and lower bounds of the effective fracture energy; marker is the mean value. (b) Comparison of the observed precursory moment release and the prediction from equation (2). Black line shows a slope of 1. Marker filling is the same as in panel a. Error bars are estimated through the upper and lower bounds of the critical nucleation length. The marker is the mean value.

Violay et al., 2013) have shown that the presence of water in the fault strongly reduces gouge production, which also seems to be the case in our experiments (Figure S2b).

4.2. Laboratory Precursory and Coseismic Moment Scaling: Experiments and Theory

The remarkable trend between u_{prec} and u_{cos} (section 3.4) raises the question of a possible scaling property between the total moment released during the precursory slip phase and the coseismic stage. In our experiments, the precursory moment (M_{p}) and the coseismic moment (M_0) are directly related to the precursory and coseismic slips and can be estimated following $M_{\mathrm{p}} = \mu.A.u_{\mathrm{prec}}$ (where μ is the shear modulus of the rock) and $M_0 = \mu.A.u_{\mathrm{cos}}$, respectively. The main assumption is that the finite fault area in our experiments can be used to estimate moment release during stick-slip cycles.

Two schools exist in the literature to estimate the moment release in the laboratory, either by correcting for an equivalent asperity (Eshelby, 1952; Walsh, 1971; Thompson et al., 2005) or by directly estimating moment assuming the experimental area that slipped (McLaskey & Lockner, 2014; Walsh, 1971). Here, we estimate M_{p} and M_0 directly from the experimental area with no additional correction (e.g., Walsh, 1971; Item S2). The remarkable scaling between u_{prec} and u_{cos} (i.e., M_{p} and M_0) observed in our experiments can be explained by nucleation theory. Considering that most of the precursory slip is related to the growth of a nucleation patch on the fault, supported by the exponential growth of the precursory slip, M_{p} can be written as

$$M_{\mathrm{p}}^{Lc} = \mu.u_{\mathrm{prec}}.L_c^2, \tag{2}$$

with L_{c} the critical nucleation length. Previous theoretical (Campillo & Ionescu, 1997; Ida, 1972; Uenishi & Rice, 2003) and experimental (Passelègue et al., 2016) studies have highlighted that, under slip weakening laws, the effective fracture energy ($G^{'}$) can be used in a small-scale yielding description to approximate the nucleation length as $L_{\mathrm{c}} = \beta.\frac{\mu\, G'}{\Delta\sigma_d^2}$, with $\Delta\sigma_d$ the earthquake's dynamic stress drop and β a coefficient close to unity (Uenishi & Rice, 2003). In our experiments, the effective fracture energy G' estimated following $G^{'} = \frac{\Delta\sigma.u_{\mathrm{cos}}}{2}$ from both static (lower bound and average values) and dynamic stress drop (upper bound and maximum possible values) of the main instability is a function of its seismic moment (Figure 3a). Such a trend was also observed in previous experimental (Nielsen et al., 2016; Ohnaka, 2010; Passelègue et al., 2016), seismological (Abercrombie & Rice, 2005), and theoretical studies (Viesca & Garagash, 2015). Using experimental values for G' (for details on the estimation of the effective fracture energy, and the associated uncertainties, the reader can refer to Nielsen et al., 2016), the precursory moment release measured during our experiments can be compared to the lower and the upper bounds predicted by nucleation theory (from equation (2) using both static and dynamic stress drops for the calculation of G', respectively; Figure 3b). The predicted precursory seismic moment M_{p}^{Lc} increases with M_{p} and is in good

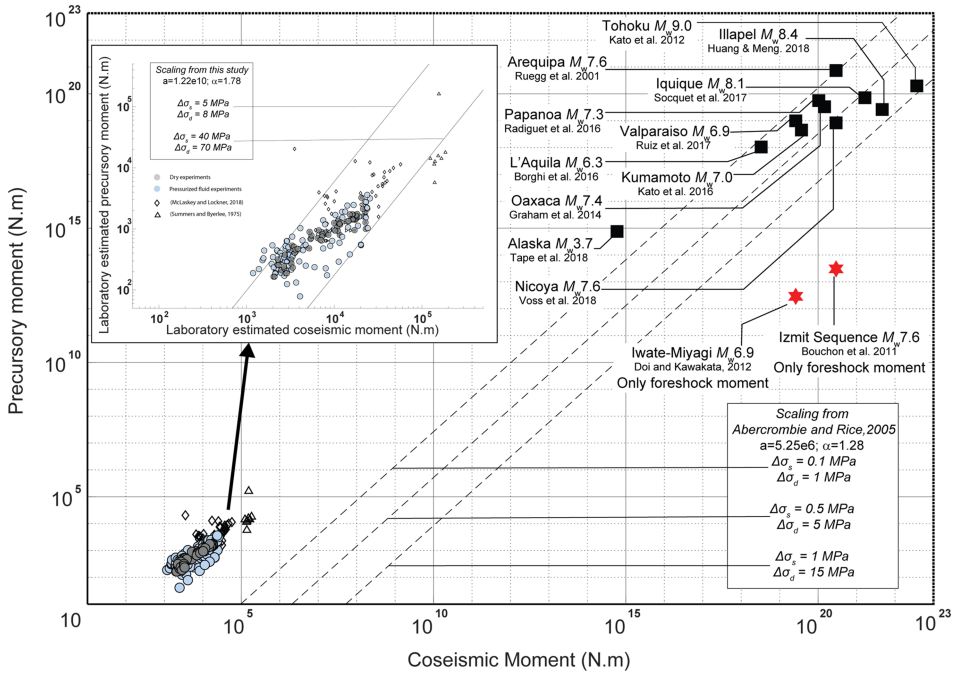

Figure 4. Precursory and coseismic moment release in natural earthquakes. Data from natural and laboratory earthquakes. Full squares account for M_p inferred from an integrated analysis of a combination of geodetic and/or seismic precursory moment release. Red stars correspond to observations of M_p estimated only from foreshock moment release. Dashed lines correspond to M_0 versus M_p from equation (6) using the scaling from Abercrombie and Rice (2005) with $\alpha = 1.28$ and $a = 5.25 \times 10^6$ and different static and dynamic stress drops. Filled circles account for M_p and M_0 from this study. Blue filling accounts for experiments in the presence of fluid pressures and gray filling for nominally dry experiments. All other symbols account for external data of laboratory experiments. Insert shows zoom on laboratory earthquakes with the scaling law (full lines). The power exponent $\alpha = 1.78$ is then inferred from the scaling between the effective fracture energy and the coseismic slip from our experiments (Figure S4a).

agreement with the experimental measurements, suggesting that (i) M_p is indeed a function of L_c (estimated from coseismic energy dissipation), (ii) L_c in our experiments is systematically close to the experimental fault length (L), and (iii) M_p increases with the earthquake's G', that is, the size of the earthquake which is eventually going to rupture (Figure 3a, color bar).

4.3. Comparison With Natural Earthquakes

While the precursory moment release remains scarcely determined in most natural seismicity, several examples of well-instrumented earthquakes seem to follow the same trend as our laboratory earthquakes and highlight that the M_p scales with the seismic moment of the mainshock (Figure 4). Note that we tried to compile as many observations as possible (to our knowledge) where the precursory nucleation phase could be resolved using geodetic analyses of modeled fault displacement prior to the mainshock (Borghi et al., 2016., Kato et al., 2016, Socquet et al., 2017; Radiguet et al., 2016; Ruiz et al., 2017; Graham et al., 2014; Voss et al., 2018) and/or aseismic fault slip inferred from earthquake repeaters and foreshocks (Bouchon et al., 2011; Huang & Meng, 2018; Kato et al., 2012; Kato et al., 2016; Ruiz et al., 2017). Therefore, Figure 4 (details in Item S3) should be considered carefully. Nonetheless, the scaling relationship could be valid when geodetic- and/or seismic-inferred measurements of precursory moment release are taken into account (Figure 4, black squares). In light of our results, when precursory aseismic slip can be resolved, existing experimental and seismological observations suggest that M_p, that is, the energy released during the nucleation phase increases with the seismic moment of the mainshock.

The question is then, can nucleation theory can be used to predict the natural observations? The prediction M_p^{Lc} (e.g., equation (2)) applied to experimental data requires measurement of the precursory slip, which is known for individual natural events, but not for a large range of seismic moments. However, u_{prec} can be replaced in equation (2) assuming that the amount of slip is a function of the stress drop released within

the slipped volume (Kanamori & Brodsky, 2004). Then, if the fault is considered as a shear crack, the static stress drop associated to the precursory event can be written: $\Delta\sigma_s = C.\mu.\frac{u_{prec}}{L_c}$, where C is a geometric constant dependent on the crack's shape; and μ, the rock's shear modulus. From these two relations, we find that the precursory moment release can be written: $M_p = \frac{L_c^3}{C}.\Delta\sigma_s$. We thus get a scaling between the precursory moment M_p, the static and dynamic stress drops, and the effective fracture energy G'.

$$M_p^{G'} = \frac{(\beta\mu G')^3}{C}.\frac{\Delta\sigma_s}{\Delta\sigma_d^6}. \quad (3)$$

Adding the additional hypothesis that u_{prec} is function of $\Delta\sigma_s$ results in additional scatter in the laboratory data as shown in Figure S4b, mainly due to the finite experimental fault area (Item S2). Note nevertheless that the theoretically predicted ${M_p}^{G'}$ remains conservative concerning laboratory earthquakes.

Experimental (Nielsen et al., 2016; Ohnaka, 2010; Passelègue et al., 2016), seismological (Abercrombie & Rice, 2005), and theoretical studies (Viesca & Garagash, 2015) demonstrated that the effective fracture energy of earthquakes increases as a power law of their coseismic slip—as shown in Figure 3a—and can be written as

$$G' = a\,{u_{cos}}^{\alpha}, \quad (4)$$

where a is a scaling prefactor and α is a given power (Figure S4a).

Then, regarding the mainshock, the coseismic static stress drop is $\Delta\sigma_s = C.\mu.\frac{u_{cos}}{L}$ (Kanamori & Brodsky, 2004). Because the seismic moment of such earthquakes is $M_0 = \mu.u_{cos}.L^2$, with L being the dimension of the ruptured asperity (here the radius), we find

$$u_{cos} = \frac{\Delta\sigma_s^{\frac{2}{3}} M_0^{\frac{1}{3}}}{\mu\, C^{\frac{2}{3}}}. \quad (5)$$

Combining equations (3)–(5), we obtain the following scaling relation between precursory and coseismic moments:

$$M_p^{M_0} = \frac{(a.\beta.\mu^{1-\alpha})^3}{C^{2\alpha+1}}.\frac{\Delta\sigma_s^{2\alpha+1}}{\Delta\sigma_d^6}.M_0^{\alpha}. \quad (6)$$

This relationship directly shows that the larger the coseismic moment of the earthquake, the larger the precursory moment expected to be released, in agreement with experimental observations and with existent natural observations. In fact, applying equation (6) with the scaling proposed by Abercrombie & Rice, 2005; equation (4) with $\alpha \sim 1.28$ and $a = 5.25 \times 10^6$) and usual earthquake stress drops ($\Delta\sigma_s \sim 0.1$–1 MPa and $\Delta\sigma_d = 1$–10 MPa; Twardzik et al., 2014), the proposed scaling provides conservative estimates for natural earthquakes (Figure 4, dotted lines). Note that laboratory experiments are underestimated by this prediction. Such discrepancy can be due (i) to the difference in static and dynamic stress drops due to finite fault area in laboratory experiments and (ii) to the different scaling power (α) with respect to natural earthquakes (lines are computed through equation (6) with $\alpha = 1.78$; Figure S4a).

Importantly, some observations fall out of the scaling law (Figure 4, red stars from Bouchon et al., 2011; Doi & Kawakata, 2012). Note that there was no significant precursory crustal deformation with amplitude greater than noise level of a tilt meter nearby the epicenter of the 2008 M_w 6.9 Iwate-Miyagi earthquake (Hirose, 2011). It is possible that in those observations (and in many other earthquakes where u_{prec} could not be resolved), the precursory moment release could not be fully detected. Another explanation is that such events presented a significantly different slip behavior (cascade-like initiation, e.g., Ellsworth & Bulut, 2018, Noda et al., 2013) prior to rupture which does not agree with the proposed scaling relationship. Further investigation of natural observations is needed to clarify which of these explanations is valid.

5. Conclusions and Implications for Natural and Anthropogenic Earthquakes

Through detailed observation of laboratory earthquake nucleation, we have observed that the temporal evolution of slip and seismicity preceding the mainshock can strongly depend on fault's fluid pressures and slip history as well as stress conditions (Passelègue et al., 2017) and fault initial roughness (Yamashita et al., 2018). Nevertheless, under all experimental conditions presented in this study, the precursory moment

release scales with the magnitude of the mainshock as predicted by a semiempirical scaling relationship (equations (3) and (6)). Such scaling relationships applied with the scaling between effective fracture energy and coseismic slip observed for natural earthquakes (Abercrombie & Rice, 2005) provide conservative estimates for existing observations of natural earthquakes of M_w 6.0 to M_w 9.0.

If this scaling relationship is correct, it can have strong implications for the earthquake nucleation phase. First, in the laboratory, the precursory moment release systematically follows an exponential growth during the first acceleration phase. If it were the case in (some) natural earthquakes, continuous monitoring of FC could provide first order information about the fault's stability and eventual rupture initiation. Note that in natural earthquakes, exponential acceleration of precursory slip has rarely been detected (Voss et al., 2018).

Second, the occurrence of a large earthquake (M_w 7.0 or higher) does not imply that a larger earthquake will not occur in the days following it. If the released seismic moment contributes to the precursory moment for a bigger asperity, a larger earthquake can occur soon after, as was the case for the 2011 M_w 9.0 Tohoku-Oki (Kato et al., 2012), the 2014 M_w 8.1 Iquique (Socquet et al., 2017), the 2016 M_w 7.0 Kumamoto (Kato et al., 2016), the 1960 M_w 9.4–9.6 Valdivia (Barrientos & Ward, 1990) and 2019 M_w 7.1 Ridgecrest earthquakes, all of which were preceded by large M_w foreshocks (Item S3).

Third, and foremost, independent of initial conditions (fluid pressure, slip history, and FC), the larger M_p, the larger the expected M_0 (Figures 3 and 4) whether it is released seismically, aseismically, or by a combination of both. In fact, the dynamic propagation of the earthquake rupture needs a given amount of elastic strain energy to be dissipated at the rupture tip (Campillo & Ionescu, 1997; Ohnaka, 2010; Uenishi & Rice, 2003). For the fault to transition from a static or quasistatic state to a dynamic propagation state, a given amount of energy needs to be dissipated, thus a given amount of precursory moment needs to be released. Therefore, if an earthquake shows a nucleation phase (exponential acceleration of slip), such a phase should be larger for a larger earthquake. Nevertheless, many earthquakes do not seem to present a nucleation phase. This confirms that both the number of foreshocks and their characteristic acceleration can differ for a given earthquake magnitude (Bouchon et al., 2011, 2013; Doi & Kawakata, 2012). Moreover, fluid pressures are likely to reduce FC (Moreno et al., 2014; Voss et al., 2018) compared to dry conditions and, in light of our experiments, regulate (detectable) foreshock sequences.

Today, natural observations of precursory moment release are still too scarce to reach a significant conclusion on whether precursory moment release scales with natural earthquake magnitudes (gap in Figure 4). Nevertheless, this study should encourage close studies of precursory moment release in seismogenic fault zones and deployment of instrumentation to this end. Furthermore, closely monitoring fault displacements in anthropogenic seismicity and decametric laboratory experiments (e.g., Guglielmi et al., 2015) could possibly shed light on the precursory mechanisms of small to moderate earthquake ruptures.

Data Availability Statement

The additional data to reproduce Figures 1 and 2 in this study can be found on the Zenodo (https://zenodo.org/deposit/3360859#) repository under deposit number 3360859. All data necessary to reproduce Figures 3 and 4 are given in Tables S1–S3 and prediction equations in the main text. All other data presented in this study are given in the supporting information.

Acknowledgments
M. A. and M. V. acknowledge the funding support from the Swiss National Science Foundation (SNF), Project PYAPP2160588, the technical staff at LEMR for help with sample preparation, and Barnaby Fryer for proofreading the manuscript. M. V. acknowledges the European Research Council Starting Grant Project 757290-BEFINE. A. S. acknowledges the European Research Council, Grant 681346-REALISM. F. X. P. acknowledges funding from the SNF, Project PZENP2173613. M. A., M. V., and A. S. also acknowledge the Germaine de Staël French-Swiss exchange program.

References

Abercrombie, R. E., & Rice, J. R. (2005). Can observations of earthquake scaling constrain slip weakening? *Geophysical Journal International*, *162*(2), 406–424. https://doi.org/10.1111/j.1365-246X.2005.02579.x

Acosta, M., Passelègue, F. X., Schubnel, A., & Violay, M. (2018). Dynamic weakening during earthquakes controlled by fluid thermodynamics. *Nature Communications*, *9*(1), 3074. https://doi.org/10.1038/s41467-018-05603-9

Barrientos, S. E., & Ward, S. N. (1990). The 1960 Chile earthquake: Inversion for slip distribution from surface deformation. *Geophysical Journal International*, *103*(3), 589–598. https://doi.org/10.1111/j.1365-246X.1990.tb05673.x

Ben-David, O., Cohen, G., & Fineberg, J. (2010). The dynamics of the onset of frictional slip. *Science*, *330*(6001), 211–214. https://doi.org/10.1126/science.1194777

Borghi, A., Aoudia, A., Javed, F., & Barzaghi, R. (2016). Precursory slow-slip loaded the 2009 L'Aquila earthquake sequence. *Geophysical Journal International*, *205*(2), 776–784. https://doi.org/10.1093/gji/ggw046

Bouchon, M., Durand, V., Marsan, D., Karabulut, H., & Schmittbuhl, J. (2013). The long precursory phase of most large interplate earthquakes. *Nature Geoscience*, *6*(4), 299–302. https://doi.org/10.1038/ngeo1770

Bouchon, M., Karabulut, H., Aktar, M., Ozalaybey, S., Schmittbuhl, J., & Bouin, M. P. (2011). Extended nucleation of the 1999 Mw 7.6 Izmit earthquake. *Science*, *331*(6019), 877–880. https://doi.org/10.1126/science.1197341

Brace, W. F., & Byerlee, J. D. (1966). Stick-slip as a mechanism for earthquakes. *Science*, *153*(3739), 990–992. https://doi.org/10.1126/science.153.3739.990

Byerlee, J. D. (1978). Friction of rocks. In *Rock friction and earthquake prediction*, (pp. 615–626). Basel: Birkhäuser.

Byerlee, J. D., Summers, R. Stable sliding preceding stick-slip on fault surfaces in granite at high pressure. *Pageoph*., 113. (1975)

Campillo, M., & Ionescu, I. R. (1997). Initiation of antiplane shear instability under slip dependent friction. *Journal of Geophysical Research*, *102*(B9), 20,363–20,371. https://doi.org/10.1029/97JB01508

Cornelio, C., Spagnuolo, E., Di Toro, G., Nielsen, S., & Violay, M. (2019). Mechanical behaviour of fluid-lubricated faults. *Nature Communications*, *10*(1), 1274. https://doi.org/10.1038/s41467-019-09293-9

Dieterich, J. H. (1978). Preseismic fault slip and earthquake prediction. *Journal of Geophysical Research*, *83*(B8), 3940–3948. https://doi.org/10.1029/JB083iB08p03940

Doi, I., & Kawakata, H. (2012). A non-accelerating foreshock sequence followed by a short period of quiescence for a large inland earthquake. *Geophysical Research Letters*, *39*, L11308. https://doi.org/10.1029/2012GL051779

Dublanchet, P. (2018). The dynamics of earthquake precursors controlled by effective friction. *Geophysical Journal International*, *212*(2), 853–871. https://doi.org/10.1093/gji/ggx438

Ellsworth, W. L., & Bulut, F. (2018). Nucleation of the 1999 Izmit earthquake by a triggered cascade of foreshocks. *Nature Geoscience*, *11*(7), 531–535. https://doi.org/10.1038/s41561-018-0145-1

Eshelby, J. D. (1952). The determination of the elastic field of an ellipsoidal inclusion, and related problems. *Proceedings of the Royal Society of London. Series A: Mathematical and Physical Sciences*, *241*(1226), 376–396.

Gomberg, J. (2018). Unsettled Earthquake Nucleation. *Nature Geoscience*, *11*(7), 463–464. https://doi.org/10.1038/s41561-018-0149-x

Graham, S. E., DeMets, C., Cabral-Cano, E., Kostoglodov, V., Walpersdorf, A., Cotte, N., et al. (2014). GPS constraints on the 2011–2012 Oaxaca slow slip event that preceded the 2012 March 20 Ometepec earthquake, southern Mexico. *Geophysical Journal International*, *197*(3), 1593–1607. https://doi.org/10.1093/gji/ggu019

Guglielmi, Y., Cappa, F., Avouac, J. P., Henry, P., & Elsworth, D. (2015). Seismicity triggered by fluid injection–induced aseismic slip. *Science*, *348*(6240), 1224–1226. https://doi.org/10.1126/science.aab0476

Hirose, K., (2011). Hi-net tiltmeter records prior to the 2008 Iwate-Miyagi inland earthquake, Report of the National Research institute for Earth Science and Disaster Prevention. Website: https://cais.gsi.go.jp/YOCHIREN/report/kaihou81/03_11.pdf. Last accessed on 17.09.2019.

Huang, H., & Meng, L. (2018). Slow unlocking processes preceding the 2015 Mw 8.4 Illapel, Chile, earthquake. *Geophysical Research Letters*, *45*, 3914–3922. https://doi.org/10.1029/2018GL077060

Ida, Y. (1972). Cohesive force across the tip of a longitudinal-shear crack and Griffith's specific surface energy. *Journal of Geophysical Research*, *77*(20), 3796–3805. https://doi.org/10.1029/JB077i020p03796

Kanamori, H., & Brodsky, E. E. (2004). The physics of earthquakes. *Reports on Progress in Physics*, *67*(8), 1429–1496. https://doi.org/10.1088/0034-4885/67/8/R03

Kato, A., Fukuda, J.'., Nakagawa, S., & Obara, K. (2016). Foreshock migration preceding the 2016 Mw 7.0 Kumamoto earthquake, Japan. *Geophysical Research Letters*, *43*, 8945–8953. https://doi.org/10.1002/2016GL070079

Kato, A., Obara, K., Igarashi, T., Tsuruoka, H., Nakagawa, S., & Hirata, N. (2012). Propagation of slow slip leading up to the 2011 Mw 9.0 Tohoku-Oki earthquake. *Science*, *335*(6069), 705–708. https://doi.org/10.1126/science.1215141

Lapusta, N., & Rice, J. R. (2003). Nucleation and early seismic propagation of small and large events in a crustal earthquake model. *Journal of Geophysical Research*, *108*(B4), 2205. https://doi.org/10.1029/2001JB000793

Latour, S., Schubnel, A., Nielsen, S., Madariaga, R., & Vinciguerra, S. (2013). Characterization of nucleation during laboratory earthquakes. *Geophysical Research Letters*, *40*, 5064–5069. https://doi.org/10.1002/grl.50974

McLaskey, G., & Lockner, D. A. (2014). Preslip and cascade processes initiating laboratory stick slip. *Journal of Geophysical Research: Solid Earth*, *119*, 6323–6336. https://doi.org/10.1002/2014JB011220

McLaskey, G. C., & Lockner, D. A. (2018). Shear failure of a granite pin traversing a sawcut fault. *International Journal of Rock Mechanics and Mining Sciences*, *110*, 97–110. https://doi.org/10.1016/j.ijrmms.2018.07.001

Métois, M., Socquet, A., & Vigny, C. (2012). Interseismic coupling, segmentation and mechanical behavior of the central Chile subduction zone. *Journal of Geophysical Research*, *117*, B03406. https://doi.org/10.1029/2011JB008736

Moreno, M., Haberland, C., Oncken, O., Rietbrock, A., Angiboust, S., & Heidbach, O. (2014). Locking of the Chile subduction zone controlled by fluid pressure before the 2010 earthquake. *Nature Geoscience*, *7*(4), 292–296. https://doi.org/10.1038/ngeo2102

Moreno, M., Rosenau, M., & Oncken, O. (2010). 2010 Maule earthquake slip correlates with pre-seismic locking of Andean subduction zone. *Nature*, *467*(7312), 198–202. https://doi.org/10.1038/nature09349

Nielsen, S., Spagnuolo, E., Violay, M., Smith, S., di Toro, G., & Bistacchi, A. (2016). G: Fracture energy, friction and dissipation in earthquakes. *Journal of Seismology*, *20*(4), 1187–1205. https://doi.org/10.1007/s10950-016-9560-1

Noda, H., Nakatani, M., & Hori, T. (2013). Large nucleation before large earthquakes is sometimes skipped due to cascade-up—Implications from a rate and state simulation of faults with hierarchical asperities. *Journal of Geophysical Research:- Solid Earth*, *118*, 2924–2952. https://doi.org/10.1002/jgrb.50211

Ohnaka, M. (2010). *The physics of rock failure and earthquakes*. Cambridge: Cambridge University Press.

Passelègue, F., Schubnel, A., Nielsen, S., Bhat, H. S., Deldicque, D., & Madariaga, R. (2016). Dynamic rupture processes inferred from laboratory microearthquakes. *Journal of Geophysical Research: Solid Earth*, *121*, 4343–4365. https://doi.org/10.1002/2015JB012694

Passelègue, F. X., Latour, S., Schubnel, A., Nielsen, S., Bhat, H.S. and Madariaga, R., Influence of fault strength on precursory processes during laboratory earthquakes. Geophys. Mon. 227, 229–242. (2017)

Radiguet, M., Perfettini, H., Cotte, N., Gualandi, A., Valette, B., Kostoglodov, V., et al. (2016). Triggering of the 2014 M w 7.3 Papanoa earthquake by a slow slip event in Guerrero, Mexico. *Nature Geoscience*, *9*(11), 829–833. https://doi.org/10.1038/ngeo2817

Rubin, A. M., & Ampuero, J. P. (2005). Earthquake nucleation on (aging) rate and state faults. *Journal of Geophysical Research*, *110*, B11312. https://doi.org/10.1029/2005JB003686

Ruegg, J. C., Olcay, M., & Lazo, D. (2001). Co-, post-and pre (?)-seismic displacements associated with the Mw 8.4 Southern Peru earthquake of 23 June 2001 from continuous GPS measurements. *Seismological Research Letters*, *72*(6), 673–678. https://doi.org/10.1785/gssrl.72.6.673

Ruiz, S., Aden-Antoniow, F., Baez, J. C., Otarola, C., Potin, B., del Campo, F., et al. (2017). Nucleation phase and dynamic inversion of the Mw 6.9 Valparaíso 2017 earthquake in Central Chile. *Geophysical Research Letters*, *44*, 10,290–10,297. https://doi.org/10.1002/2017GL075675

Ruiz, S., Metois, M., Fuenzalida, A., Ruiz, J., Leyton, F., Grandin, R., et al. (2014). Intense foreshocks and a slow slip event preceded the 2014 Iquique Mw 8.1 earthquake. *Science*, *345*(6201), 1165–1169. https://doi.org/10.1126/science.1256074

Savage, J. C. (1983). A dislocation model of strain accumulation and release at a subduction zone. *Journal of Geophysical Research*, *88*(B6), 4984–4996. https://doi.org/10.1029/JB088iB06p04984

Scholz, C., Molnar, P., & Johnson, T. (1972). Detailed studies of frictional sliding of granite and implications for the earthquake mechanism. *Journal of Geophysical Research*, *77*(32), 6392–6406. https://doi.org/10.1029/JB077i032p06392

Socquet, A., Valdes, J. P., Jara, J., Cotton, F., Walpersdorf, A., Cotte, N., et al. (2017). An 8-month slow slip event triggers progressive nucleation of the 2014 Chile megathrust. *Geophysical Research Letters*, *44*, 4046–4053. https://doi.org/10.1002/2017GL073023

Summers, R., Byerlee, J.D., Summary of results of frictional sliding studies at confining pressures up to 6.98 kb. in selected rock materials., *U.S. Geol. Surv*. Open File Rep., 129, 77-142. (1977). https://doi.org/10.3133/ofr77142

Tape, C., Holtkamp, S., Silwal, V., Hawthorne, J., Kaneko, Y., Ampuero, J. P., et al. (2018). Earthquake nucleation and fault slip complexity in the lower crust of central Alaska. *Nature Geoscience*, *11*(7), 536–541. https://doi.org/10.1038/s41561-018-0144-2

Thompson, B. D., Young, R. P., & Lockner, D. A. (2005). Observations of premonitory acoustic emission and slip nucleation during a stick slip experiment in smooth faulted Westerly granite. *Geophysical Research Letters*, *32*, L10304. https://doi.org/10.1029/2005GL022750

Twardzik, C., Das, S., & Madariaga, R. (2014). Inversion for the physical parameters that control the source dynamics of the 2004 Parkfield earthquake. *Journal of Geophysical Research: Solid Earth*, *119*, 7010–7027. https://doi.org/10.1002/2014JB011238

Uenishi, K., & Rice, J. R. (2003). Universal nucleation length for slip-weakening rupture instability under nonuniform fault loading. *Journal of Geophysical Research*, *108*(B1), 2042. https://doi.org/10.1029/2001JB001681

Viesca, R. C., & Garagash, D. I. (2015). Ubiquitous weakening of faults due to thermal pressurization. *Nature Geoscience*, *8*(11), 875–879. https://doi.org/10.1038/ngeo2554

Violay, M., Nielsen, S., Spagnuolo, E., Cinti, D., Di Toro, G., & Di Stefano, G. (2013). Pore fluid in experimental calcite-bearing faults: Abrupt weakening and geochemical signature of co-seismic processes. *Earth and Planetary Science Letters*, *361*, 74–84. https://doi.org/10.1016/j.epsl.2012.11.021

Voss, N., Dixon, T. H., Liu, Z., Malservisi, R., Protti, M., & Schwartz, S. (2018). Do slow slip events trigger large and great megathrust earthquakes? *Science Advances*, *4*(10). https://doi.org/10.1126/sciadv.aat8472

Walsh, J. B. (1971). Stiffness in faulting and in friction experiments. *Journal of Geophysical Research*, *76*(35), 8597–8598. https://doi.org/10.1029/JB076i035p08597

Wang, X. Q., Schubnel, A., Fortin, J., Guéguen, Y., & Ge, H. K. (2013). Physical properties and brittle strength of thermally cracked granite under confinement. *Journal of Geophysical Research: Solid Earth*, *118*, 6099–6112. https://doi.org/10.1002/2013JB010340

Yabe, S., & Ide, S. (2018). Variations in precursory slip behavior resulting from frictional heterogeneity. *Progress in Earth and Planetary Science*, *5*(1), 43. https://doi.org/10.1186/s40645-018-0201-x

Yamashita, F., Fukuyama, E., Xu, S., Mizoguchi, K., Kawakata, H., & Takizawa, S. (2018). Rupture preparation process controlled by surface roughness on meter-scale laboratory fault. *Tectonophysics*, *733*, 193–208. https://doi.org/10.1016/j.tecto.2018.01.034